IJEMD-BMCR, 1 (1) (2023), 1 – 16 https://doi.org/10.54938/ijemdbmcr.2023.01.1.213

IJEMD

International Journal of Emerging Multidisciplinaries:

Biomedical and Clinical Research

Research Paper

Journal Homepage: www.ojs.ijemd.com

ISSN (print): 2957-8620 ISSN (online): 2960-0731

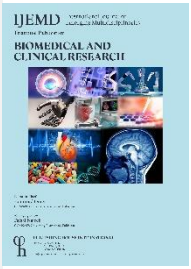

GROG-pCS: GRAPPA Operator Gridding with CS-based p-thresholding for Under-sampled Radially Encoded MRI

Fariha Aamir[1], Husnain Javid Bhatti[1], and Ibtisam Aslam[1,2], Faisal Najeeb[1*], Hammad Omer[1]

[1]Medical Image Processing Research Group (MIPRG), Department of Electrical and Computer Engineering, COMSATS University Islamabad (CUI), Pakistan

[2]Department of Radiology and Medical Informatics, Hospital University of Geneva, Switzerland

**Corresponding Author*

Abstract

Major limitation of MRI is long scan time. Compressed Sensing (CS) is a contemporary technique used to accelerate MRI scan time. In CS, fully sampled MRI images are reconstructed from the partially acquired *k*-space data. In CS MRI, the utilization of a non-linear reconstruction algorithm is one of the key requirements for successful signal recovery. Numerous methods have been used in CS for solving the non-linear problems to get the solution image. In this paper, we proposed GRAPPA Operator gridding (GROG) with CS-based p-thresholding to reconstruct the artifact free MR images from the partially acquired radial *k*-space data. In this proposed scheme, initially radially acquired under-sampled *k*-space data is mapped onto Cartesian space using GROG gridding and then CS reconstruction is performed by using iterative *p*-thresholding. The proposed method is tested on four MRI data sets, (i) simulated Shepp-Logan phantom, (ii) 1.5T human brain data, (iii) 3T human brain, and (iv) 3T short-axial cardiac (SA) radial data. The reconstruction results are compared with the CS-based iterative hard-thresholding and soft-thresholding reconstructions. The quality of the solution images is evaluated by using (i) Artifact Power (AP), (ii) Root Mean Square Error (RMSE), and (iii) Peak Signal-to-Noise Ratio (PSNR).

Keywords: Compressed Sensing; GRAPPA; GROG; MRI Image Reconstruction; Phantom; p-thresholding; Soft Thresholding

Email addresses: farihaaamir23@gmail.com (Fariha Aamir), hussnain_j@yahoo.com (Husnain Javid Bhatti), ibtisam.aslam@comsats.edu.pk (Ibtisam Aslam), faisal.86n@gmail.com (Faisal Najeeb), hammad.omer@comsats.edu.pk (Hammad Omer)

1. Introduction

MRI is a non-ionizing medical imaging technique that utilizes magnetic field and radio waves to generate better quality images of the human body [1]. The key factor of MRI is an excellent soft-tissue contrast, better than other contemporary medical imaging techniques e.g., X-ray, CT, PET etc. [2-4]. Long scanning time is a major limitation of MRI which can be perturbing for the patients [5]. MRI scan time can be decreased via under-sampled *k*-space, but the subsequent images may have artifacts [6]. From the under-sampled data, numerous methods have been introduced in the literature to reconstruct the un-aliased images e.g. SENSE[3], GRAPPA [4], ESPIRiT [5].

Non-Cartesian (NC) trajectories play an important role in achieving faster scanning in MRI but the resultant images may contain complex artifacts [7-11]. NC trajectories help to minimize the acquisition time but require an extra post-processing called gridding. Gridding maps the acquired NC data onto a Cartesian grid before the inverse Fast Fourier Transform (IFFT) to obtain the MR image. Different gridding methods have been proposed to sample the acquired NC data onto a Cartesian grid e.g. Convolution gridding [7], Fessler gridding [8], and GRAPPA Operator Gridding (GROG) [9].

Convolution gridding [7] (the most used method for gridding) maps the attained NC data onto the Cartesian matrix by interpolating the acquired data with Kaiser–Bessel window followed by Density Compensation Function (DCF). The non-uniform FFT (NUFFT) introduced by Fessler [8] utilizes the min-max interpolation to converts the non-Cartesian data onto a Cartesian space followed by DCF. Besides, both conventional gridding (Fessler and convolutional) methods require additional parameters e.g interpolation kernel with various sizes, shapes and DCF [10–12].

N. Seblerich et.al [9] proposed GRAPPA Operator gridding (GROG) to transfer the acquired NC data samples to the Cartesian grid. Each acquired NC data point is mapped via GROG to the neighboring Cartesian location by employing self-calibrated multi-coil weight sets; however, some unfilled spaces are present in the gridded data. One advantage of GROG over conventional gridding [7,8] techniques is that it does not require any extra gridding factors like kernel and DCF.

Compressed Sensing (CS) [13] is a trending approach for MR image reconstruction that efficiently recovers the solution image from fewer *k*-space samples. There are some requirements for successful CS based MR image reconstruction: (i) data must be sparse (ii) image should contain incoherent artifacts (iii) the reconstruction technique should be non-linear. In the recent past, different algorithms have been applied for CS-based image reconstruction such as non-linear conjugate Gradient (NLCG), iterative hard thresholding Algorithm (IHTA), iterative soft thresholding algorithm (ISTA) [14,15] and iterative *p*-thresholding algorithm [12]. Iterative thresholding methods [15] are a developing area of interest in CS signal recovery.

This paper proposes an application of ‘GROG followed by iterative *p*-thresholding based CS (GROG-pCS)’ to reconstruct the MR images from the acquired non-Cartesian (radial) under-sampled *k*-space data. The outcomes of the proposed method are compared to the two conventional CS reconstruction techniques IHTA and ISTA [16].

Theory

GROG Gridding

N. Seiberlich et.al.[9] proposed GROG to map the NC samples to the nearby Cartesian locations utilizing coil-by-coil self-calibrated weight sets. GROG moves each NC sample to the nearby Cartesian location by a shift, both in *x* and *y* directions, i.e. Δk_x and Δk_y:

$$\boldsymbol{s\left(k_x + \Delta k_x, k_y + \Delta k_y\right) = G_z \,.\, s(k_x\,, k_y)} \qquad (1)$$

In equation (1), $s(k_x\,, k_y)$ is the acquired NC point for a two-dimensional case; G_z is the weight matrix with dimensions $N_c \times N_c$; where N_c represents the number of receiver channels and $s\left(k_x + \Delta k_x\,, k_y + \Delta k_y\right)$ is the estimated signal at the adjacent Cartesian position.

GROG is a worthwhile gridding procedure as it does not require any density compensation function (DCF), kernel size, and shape. GROG leaves a few unfilled positions in the gridded Cartesian *k*-space that enhances data sparsity and makes GROG gridding feasible for CS [14] based image reconstruction.

Summary of Iterative Thresholding Techniques in CS-MRI

CS [13] is used to recover the un-aliased MR images from the partially acquired *k*-space data, thereby considerably decreasing the MRI examination time. Generalized optimization of MR image reconstruction problem based on CS can be written in the Lagrangian notation as:

$$\boldsymbol{min_m ||F_u m - y||_2^2 + \lambda \|\Psi m\|_1} \qquad (2)$$

where F_u is the Fourier transform operator, m represents the sparse coefficient of the final image, y is the scanner acquired data, λ represents the thresholding factor and Ψ is taken as a sparsifying transform. In the above expression, the first term is used for error minimization and the second term is used to enforce sparsity.

Iterative thresholding in CS is a developing area in which the de-aliased MR image can be obtained from the acquired under-sampled data [18-19]. Recently, Thomas Blumensath [20] proposed iterative hard-thresholding algorithm (IHTA) for the CS-MR recovery problem from the uniformly under-sampled data. However, hard-thresholding sometimes allows pure noise coefficients that may appear in the reconstructed image. Hard-thresholding operator is defined as:

$$\boldsymbol{H_\lambda(\beta_i) = \begin{cases} \beta_i, & |\beta_i| > \lambda \\ 0, & |\beta_i| \le \lambda \end{cases}} \qquad (3)$$

In Equation (3), H is the thresholding function, β_i is the i^{th} element in the sparse data and λ is the thresholding factor. Hard-thresholding may provide some discontinuities in the resultant image[20-21].

Xiaobo et.al. [20] proposed an iterative soft thresholding algorithm (ISTA) for 1D variable density under-sampled Cartesian trajectory-based CS-MR image reconstruction. ISTA solves the CS image

reconstruction problem when the solution is sparse enough. ISTA is an extension of IHTA and shrinks the noise coefficient above the threshold values. Soft-thresholding is defined as [20]:

$$S_{\lambda}(\beta_i) = \begin{cases} \beta_i + \lambda, & \beta_i \leq -\lambda \\ 0, & \beta_i < \lambda \\ \beta_i - \lambda, & \beta_i \geq 0 \end{cases} \quad (4)$$

In Equation (4), S is the thresholding function, β_i is the i^{th} element in the sparse data and λ is the thresholding factor. ISTA converges with a linear rate as compared to other thresholding techniques.
p-thresholding [19] is a variant of ISTA that has been recently proposed to minimize the ℓ_1-constrained problem and retrieves the artifact-free MR image iteratively. the *p*-thresholding operator is defined as:

$$(X_p(m))_k = [sign\,(m_k).max\,\{0,\ |m|_k - \lambda|m|_k^{p-1}] \quad (5)$$

In equation (5), X signifies thresholding function, λ represents the factor of thresholding, a weight factor is added to the coefficients of m defined by p, m represents the resultant image and $sign$ is a signum function. In this technique, p is an additional parameter that adjusts itself with different values to get different thresholding techniques e.g., ISTA and IHTA.

GROG followed by iterative *p*-Thresholding based CS (GROG-pCS: Proposed Method)

In this paper a novel approach 'GROG followed by CS-based *p*-thresholding (GROG-Pcs)' is proposed to obtain the de-aliased MR images from the radially under-sampled *k*-space data.

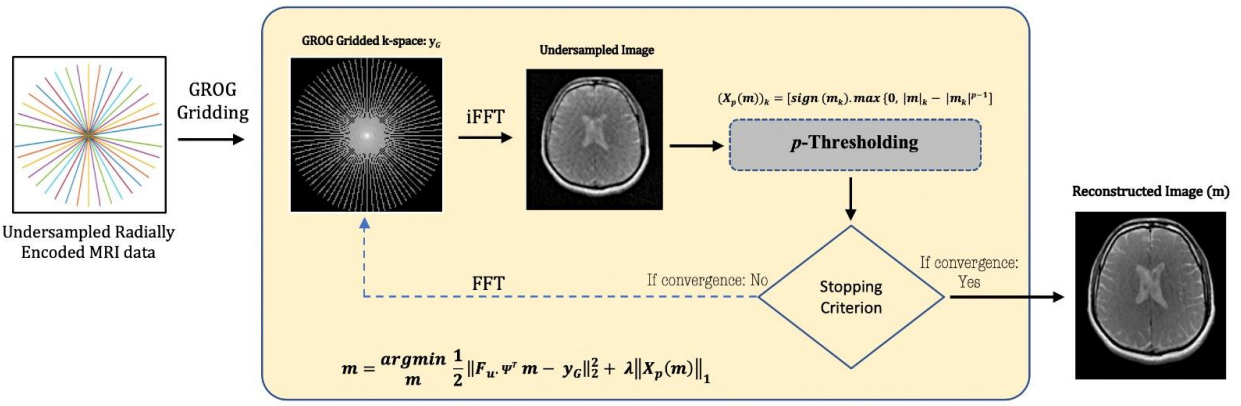

Fig. 1: A schematic depiction of the proposed method (GROG-pCS). Initially, under sampled radially encoded MRI data is converted to a Cartesian grid by using GROG gridding. Then iterative CS based *p*-thresholding is applied to obtain the artifact recovered MR image.

The proposed technique reconstructs the MR image in two stages: (i) GROG gridding is used to convert the acquired non-Cartesian (radial) *k*-space data to the Cartesian locations and (ii) iterative CS based *p*-thresholding is applied to obtain the artifact recovered MR image.

In the proposed scheme, the acquired radial data is initially mapped to the Cartesian scheme using GROG (equation (6)):

$$\boldsymbol{y_G = G.y} \qquad \textbf{(6)}$$

where y is the acquired multi-channel radial *k*-space data from the scanner, G signifies the GROG gridding and y_G being the GROG gridded data.

As GROG gridded data has missing points that increase the data sparsity, so CS-based iterative *p*-thresholding is a good choice to recover the solution MR images. Since GROG leaves void positions in the gridded *k*-space [13], therefore, the subsequent iterative reconstruction and data consistency can be implemented directly in the Cartesian domain that significantly decreases the computation time of the proposed scheme.

A CS-MRI optimization equation is utilized to solve the MR reconstruction problem which includes the *k*-space data consistency constraints and sparsity presented by the accompanying Lagrangian limit as:

$$\boldsymbol{m = \underset{m}{argmin}\ \frac{1}{2}\|F_u.\Psi^T\, m - \ y_G\|_2^2 + \ \lambda\left\|X_p(m)\right\|_1} \qquad (7)$$

where, F_u represents the sub-sampled Fourier transform, m being the sparse coefficient of the solution image (m= Ψz; where z is IFFT of under-sampled *k*-space data), X_p is the thresholding function, Ψ is taken as sparsifying transform (wavelet in this work), λ is the thresholding parameter and y_G is the GROG gridded *k*-space data. In equation (7), the first part is the data fidelity term that shows the error minimization, and the second term represents the *p*-thresholding as an ℓ_1 constraint. CS-based *p*-thresholding for the ℓ_1 the constraint reconstruction problem is defined as:

$$\boldsymbol{(X_p(m))_k = [sign\,(m_k).max\,\{0,\ |m|_k - \ |m_k|^{p-1}]} \quad \textbf{(8)}$$

where, X_p is the thresholding function, m is the reconstructed image, p adds weight to the coefficients of m and λ is the thresholding parameter. In this work, the value of λ (λ= 0.001) is empirically chosen, following a decaying update for each iteration by the factor β to solve equation 8 where $0 < \beta < 1$. Table 1 shows the proposed method's pseudo code.

Table 1. Pseudo code of the proposed algorithm (GROG-pCS)

Pseudo Code for Proposed Method

Input

y: acquired multi-channel radial k-space

y_r : Residual

G: GROG gridding

y_G: GROG gridded k-space data

F_u: sub-sampled Fourier transform

m: sparse coefficient of the solution image

X_p: thresholding function

Ψ : sparsifying transform

λ: thresholding parameter

Initialization:

k=1, p= -2.5, λ=0.1

For $\frac{|y_r|_2}{|y_G|_2} > \varepsilon$

Compute residual $y_{r+1} = y - F_u.\Psi^T m_k$

Update coefficients $m_{k+1} = X_{p,\lambda_k}(m_k + (F_u.\Psi^T)^T.y_{r+1})$

Update threshold value $\boldsymbol{\lambda}_{k+1} = p\,\boldsymbol{\lambda}_k$

$k = k + 1$

end

Output

Reconstructed image $r_m = \Psi^T m$

Materials and Method

The proposed GROG-pCS technique retrieves the solution image from GROG gridded sub-sampled data followed by CS-based iterative *p*-thresholding. The reconstruction results are compared to two contemporary thresholding techniques, one is iterative hard-thresholding (IHTA) and the other is iterative soft-thresholding (ISTA) [20-23] schemes. In this work, the values of λ and p are chosen empirically after performing experiments for a range of values of p [i.e., 2.5 to -2.5] and λ [i.e., 0.1 to 0.05×10^{-3}]. The proposed method is implemented on MATLAB (Math Works, R2019a) and tested on four datasets, (i) Shepp–Logan phantom data, (ii) 1.5T human brain data, (iii) 3T human brain data, and (iv) 3T free breathing human short-axis (SA) cardiac radial datasets.

Data Acquisition:

We used four data sets to evaluate the performance of our proposed method. Datasets 1 [23] and 3 [25] are publicly available while written consent was obtained for datasets 2 and 4. First dataset was 8 channel Shepp–Logan phantom having dimensions $256 \times 256 \times 8$. This data was simulated on MATLAB (Math Works, R2019a) by using Biot–Savart method [23].
2nd dataset was 1.5T human head MRI data having dimensions $256 \times 256 \times 8$. This dataset was obtained at Saint Mary's Hospital, London [25]. The data was acquired with eight-channel human head coils with these examination factors: TR=500 msec, TE=10 msec, FOV=20 cm, slice thickness=3 mm, flip angle=$50^{\circ}$and matrix size=256 × 256.
The 3rd dataset was MRI human head acquired by using a 3T scanner (Waukesha, Wisconsin, USA) with eight-channel head coils. The following parameters were used for data acquisition: TR=500msec, TE=10msec, FOV=20cm, slice thickness=3mm, bandwidth=31.25 kHz/pixel, and flip angle =50^0 (publicly available and downloaded from http://www.acsu.buffalo.edu/~leiying/cbil/index.html**).**
Using the Fessler toolbox [11], Dataset-1 (Shepp–Logan phantom) and Dataset-2 (human head MRI data) were initially transformed to a fully sampled radial *k*-space with 402 radial spokes utilizing the formula : $\frac{\pi}{2} \times N$ [15], where N is the readout point. This fully sampled radially encoded data was under-sampled retrospectively at various acceleration factors ($4 \leq AF \leq 9$) to test the viability of the proposed scheme.
Experiments were also performed on another non-ECG gated, cardiac radial dataset which was acquired during free-breathing (Dataset-4). This data was radially obtained from 3T Skyra Siemens Scanner at Case Western University, USA with 30 channel and the accompanying sweep parameters: TR=2.94 ms, readout points=256 and fully sampled radial projections=144.

Evaluation Parameters
The performance of proposed method is assessed by using (i) Peak Signal-to-Noise Ratio (PSNR), (ii) Artifact Power (AP) and (iii) Root Mean Square Error (RMSE) [19-22].

AP
AP is defined as the square difference between the reference image and the reconstructed image. A lower artifact power value shows better quality of the image. AP can be calculated as [19] :

$$\boldsymbol{AP} = \frac{\sum \|\boldsymbol{I_{ref}} - \boldsymbol{I_{recon}}\|^2}{\sum |\boldsymbol{I_{ref}}(\boldsymbol{x},\boldsymbol{y})|^2} \qquad \textbf{(9)}$$

In Equation 9, I_{ref} and I_{recon} are the reference and the reconstructed images, respectively.

RMSE

RMSE [16] is based on the Mean Square Error (MSE). A lower value of RMSE represents improved image quality. RMSE is calculated as follows [1,19,22]:

$$\boldsymbol{RMSE} = \sqrt{\frac{\sum\left\|\boldsymbol{I_{ref}} - \boldsymbol{I_{recon}}\right\|^2}{\sum|\boldsymbol{I_{ref}}(\boldsymbol{x},\boldsymbol{y})|}} \qquad (\mathbf{10})$$

All parameters are same as defined in equation (9).

PSNR

PSNR is the ratio of the maximum signal strength to the noise level in the reconstructed image. A greater value of PSNR shows better signal strength, therefore better image quality. PSNR is calculated as

$$\mathbf{PSNR} = \mathbf{10}\log_{\mathbf{10}}\left(\frac{\max(\boldsymbol{I_{recon}})^2}{\boldsymbol{MSE}}\right) \qquad (\mathbf{11})$$

Similarly, MSE can be calculated as [22]:

$$\boldsymbol{MSE} = \frac{\sum\left\|\boldsymbol{I_{ref}}(\boldsymbol{x},\boldsymbol{y}) - \boldsymbol{I_{recon}}(\boldsymbol{x},\boldsymbol{y})\right\|^2}{\sum|\boldsymbol{I_{ref}}(\boldsymbol{x},\boldsymbol{y})|} \qquad \mathbf{(12)}$$

Here max finds the maximum intensity of the image, MSE signifies the mean square error and I_{recon} indicates the reconstructed image.

Results

The reconstructed images from the proposed method (GROG-pCS), CS-based hard-thresholding and CS-based soft-thresholding for all four datasets (Shepp-Logan phantom data, 1.5T & 3T brain, and 3T SA radial data) are presented in Figs. 2 to 5 respectively; where Row-A shows results from the proposed approach (GROG-pCS), Row-B shows images of the CS-based ISTA and Row-C illustrates the reconstructed images of the CS-based IHTA with 101, 67 and 45 radial lines respectively, at various AFs. In each fig, the top left corner shows the acceleration factor (AFs), and the top right corner shows the number of acquired radial projections in each data set.

Fig. 2 demonstrates the results using different thresholding techniques for dataset-1(Shepp–Logan phantom data). Fig.3 demonstrates the results using different thresholding techniques for 1.5 T human head data. The results show that at higher AF, the proposed method gives improved results while CS-based ISTA and IHTA contains more aliasing artifacts. Fig.5 shows the solution images of the proposed method, soft-thresholding (ISTA) and hard-thresholding (IHTA) for 3T cardiac SA dataset.

Tables 2-5 provides comparison of AP, RMSE and PSNR of the proposed method, soft-thresholding (ISTA) and hard-thresholding (IHTA) for all datasets.

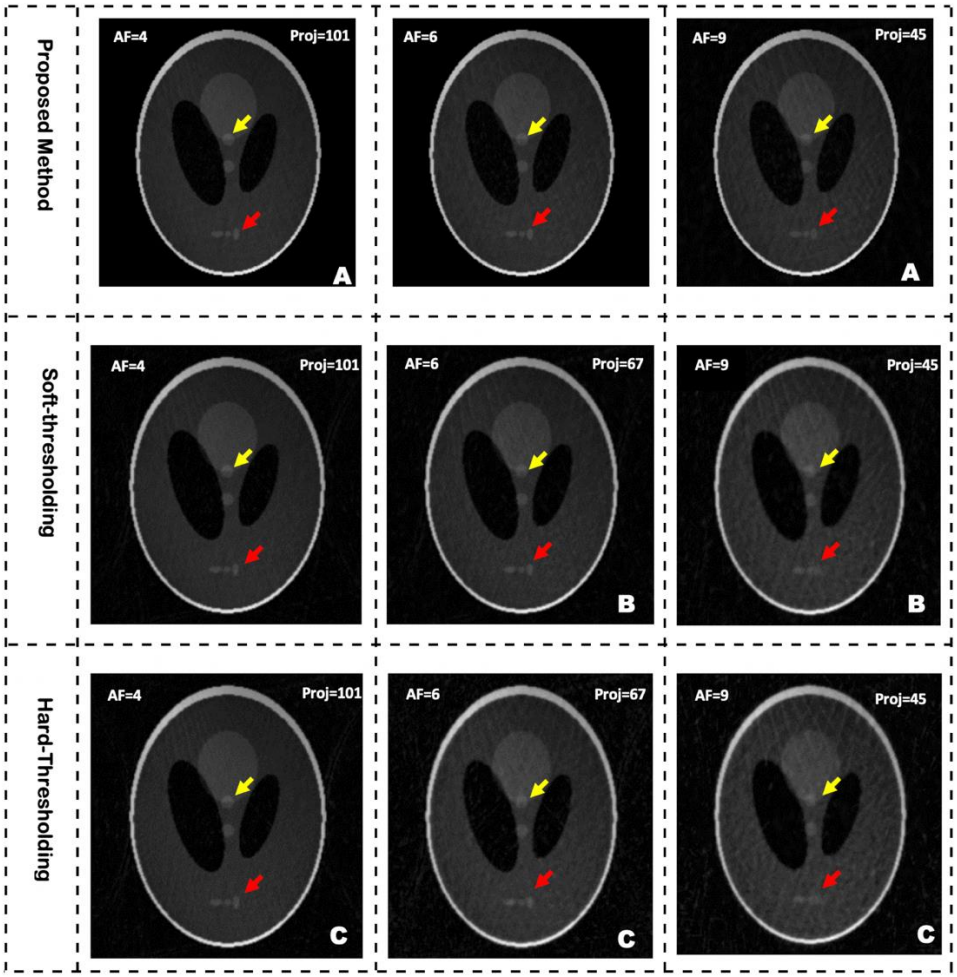

Fig.2: Simulated phantom data reconstruction results using the Proposed method, CS-based soft thresholding (ISTA) and hard thresholding (IHTA) at AF=4,6 and 9 with 101, 67, and 45 radial lines, respectively. Proposed method significantly reduces the undersampling artifacts (shown by yellow and red arrows at different location) conventional ISTA and IHTA reconstruction methods at AF=4 ,6 and 9

Table 2 AP, PSNR, and RMSE values of the proposed technique, CS-based soft and hard thresholding for the simulated phantom data. There is significant improvement in AP, RMSE and PSNR values of the proposed method compared to conventional soft and hard thresholding methods

	Proposed Method (GROG-pCS)			Soft Thresholding			Hard Thresholding		
Acceleration Factor	AP	RMSE	PSNR	AP	RMSE	PSNR	AP	RMSE	PSNR
AF = 4	0.0108	0.0297	84.2498	0.0470	0.0313	78.2556	0.0505	0.0331	77.7586
AF = 6	0.0117	0.0348	83.9876	0.0509	0.0509	77.7308	0.0711	0.0611	73.8694
AF = 9	0.0186	0.0409	81.9725	0.0585	0.0587	76.0338	0.0811	0.0683	73.4869

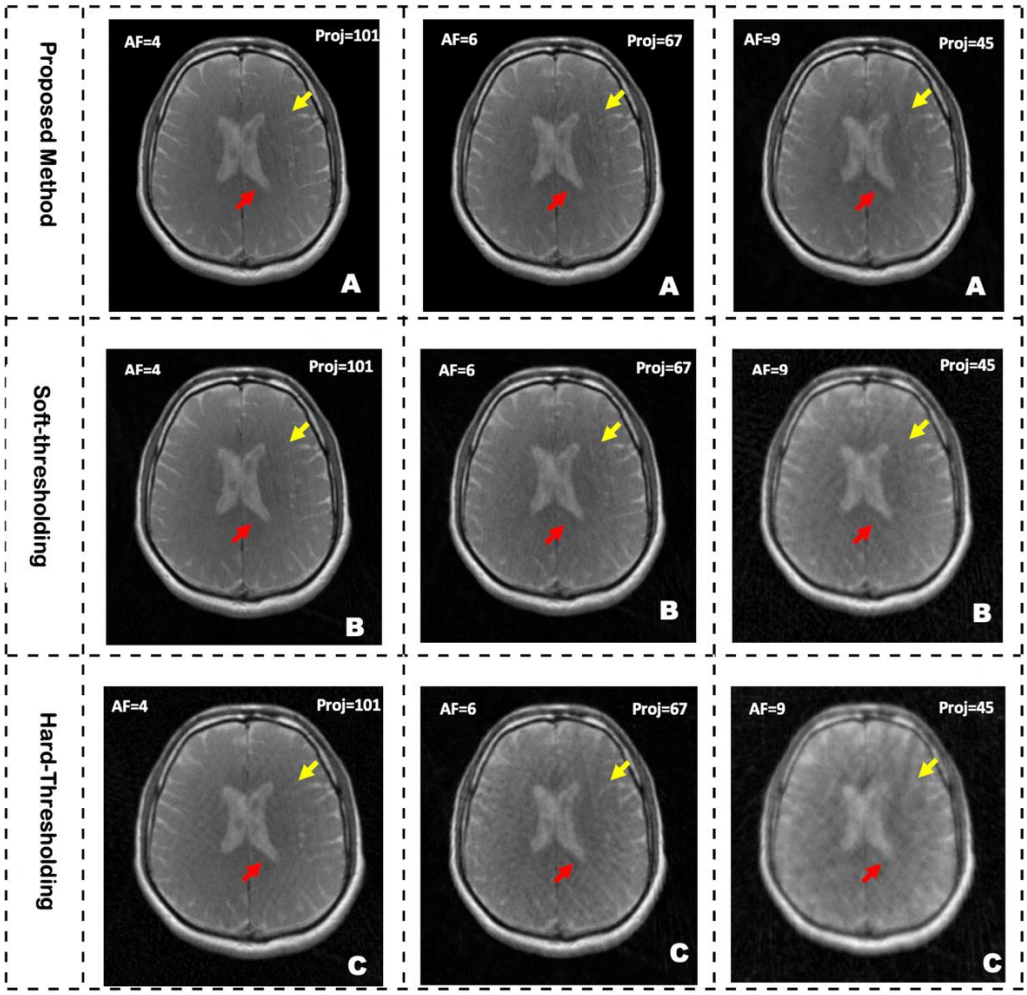

Fig.3: Results of the 1.5T human head dataset at different acceleration factors. Proposed method provides improved reconstruction results (shown by yellow and red arrows at different location) as compared to conventional CS-based ISTA and CS-based IHTA at AF=4,6. At acceleration factor=9, proposed method provides less undersampling artifacts compared to both conventional iterative thresholding techniques

Table 3 Evaluation parameters (i.e., AP, PSNR, and RMSE) of the proposed scheme, soft-thresholding and hard- thresholding-based CS for 1.5T human head reconstructed images

	Proposed Method (GROG-pCS)			Soft Thresholding			Hard Thresholding		
Acceleration Factor	AP	RMSE	PSNR	AP	RMSE	PSNR	AP	RMSE	PSNR
AF = 4	0.0042	0.0162	83.8825	0.0067	0.0204	81.9714	0.0191	0.0369	77.7586
AF = 6	0.0053	0.0189	82.6350	0.0106	0.0269	79.5848	0.0472	0.0627	73.8694
AF = 9	0.0106	0.0301	79.5765	0.0266	0.0411	75.8552	0.0852	0.0919	73.4869

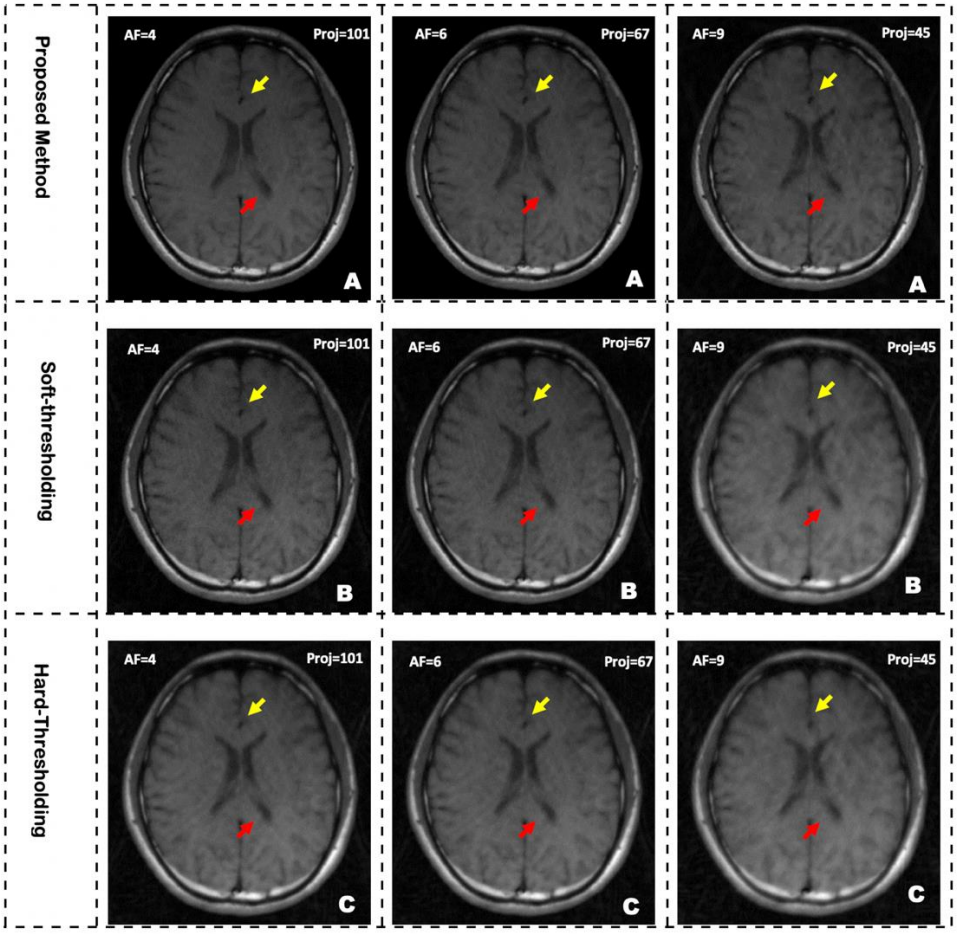

Fig.4: Results for 3T human head dataset showing a comparison of the proposed scheme with conventional soft-thresholding and hard-thresholding based CS at AF=4, 6 and 9. Proposed method provides improved reconstruction results (shown by yellow and red arrows at different location) as compared to conventional CS-based ISTA and CS-based IHTA at AF=4, 6 and 9.

Table 4 Evaluation parameters (i.e., PSNR, and RMSE) of the proposed method, soft-thresholding and hard- thresholding-based CS for 3T human head reconstructed images

	Proposed Method (GROG-pCS)			Soft Thresholding			Hard Thresholding		
Acceleration Factor	AP	RMSE	PSNR	AP	RMSE	PSNR	AP	RMSE	PSNR
AF = 4	0.0061	0.0157	84.2367	0.0191	0.0307	78.4340	0.0535	0.0575	73.0004
AF = 6	0.0078	0.0179	83.0997	0.0194	0.0309	78.3600	0.0530	0.0570	73.0428
AF = 7	0.0126	0.0266	80.6239	0.0753	0.0917	73.5432	0.0768	0.0841	69.8962

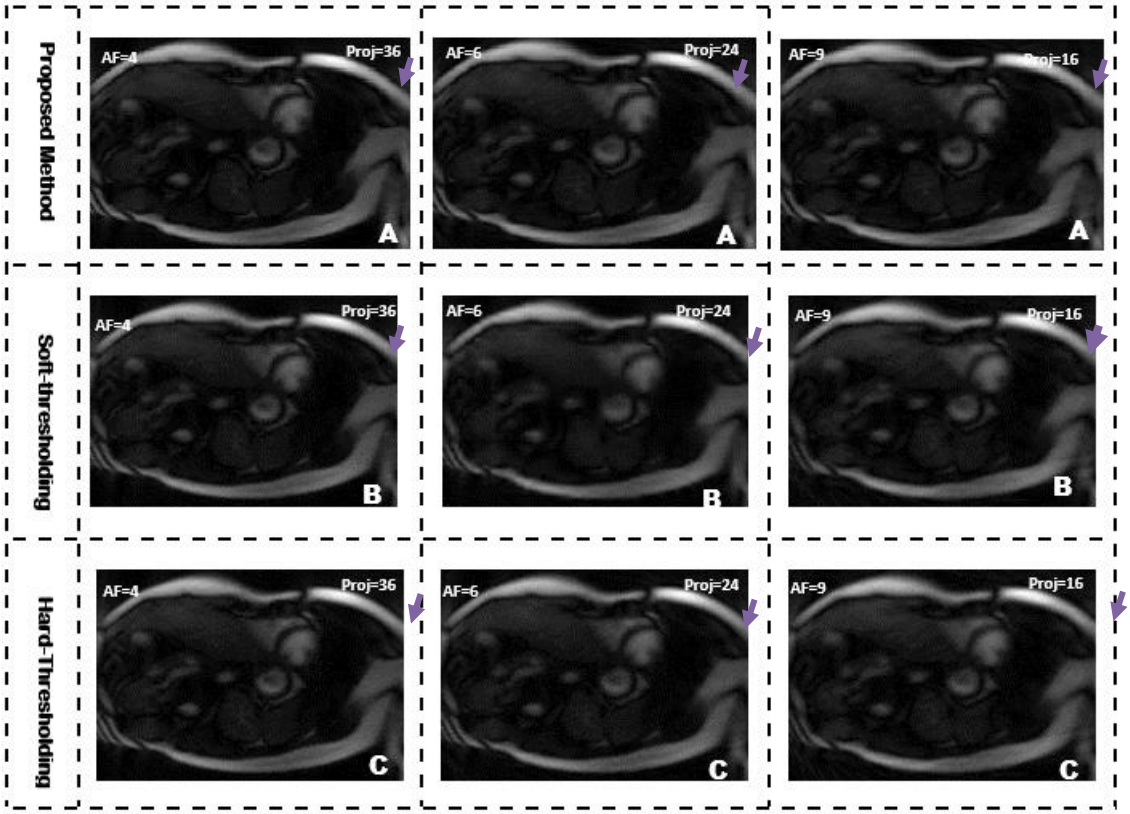

Fig.5: 3T short-axis cardiac real time radial dataset results, showing a comparison of the proposed scheme with the conventional soft-thresholding and hard-thresholding (Row-A, B and C respectively) based CS at acceleration factors $4 \leq AF \leq 9$

Table 5: AP, PSNR and RMSE values of the proposed method, soft and hard-thresholding for 3T cardiac data.

	Proposed Method (GROG-pCS)			Soft Thresholding			Hard Thresholding		
Acceleration Factor	AP	RMSE	PSNR	AP	RMSE	PSNR	AP	RMSE	PSNR
AF = 4	0.0818	0.0215	79.7653	0.0956	0.0296	78.7138	0.0956	0.0296	77.7436
AF = 6	0.0901	0.0245	78.8191	0.0923	0.0297	78.6598	0.0948	0.0298	73.6445
AF = 9	0.0977	0.0300	78.2976	0.0992	0.0316	78.2058	0.0993	0.0321	78.2304

Discussion

NC trajectories help to reduce MR examination time and under-sampling can provide a further reduction in scan time [9]. However, under-sampling results in aliasing artifacts in the final images. The radial trajectory allows the reconstruction of MR images from a restricted number of projections with a much-improved image quality compared to the Cartesian trajectories, although a further step called gridding is required as part of the image reconstruction process. Gridding resamples the acquired NC data onto a Cartesian *k*-space [10].

CS has been recently proposed for efficiently recovering the solution image from a lesser number of *k*-space samples. In this paper, GROG followed by iterative *p*-thresholding is presented to reconstruct un-aliased MR images from the acquired under-sampled radially encoded *k*-space data [9]. The results of the proposed scheme are compared to other contemporary CS based approaches for iterative MR image reconstruction i.e., CS-based ISTA and IHTA. Experiments are performed on four different radially encoded data sets with different AFs i.e. ($4 \leq AF \leq 9$), and having radial spokes 101, 67, and 45, respectively. Tables 2 to 5 provide a quantitative comparison of the evaluation parameters i.e., AP, RMSE, and PSNR values for the reconstructed images.

Table 2 shows comparison of AP, RMSE and PSNR between the proposed method, CS-based soft and hard-thresholding at different AFs for simulated phantom (dataset1) which clearly shows improvement 77% improvement with reference to soft-thresholding based CS and 78 % improvement with reference to the hard-thresholding based CS at AF=4 in terms of AP. Similarly, Table 3 provides comparison of AP, RMSE and PSNR values for all three reconstruction schemes for 1.5 T Human head data. It shows 60% improvement in AP with reference to ISTA based CS and 87% improvement with reference to the IHTA based CS at AF=9. In terms of RMSE, 26% and 67% improvements are obtained as compared to the ISTA and IHTA respectively for 1.5 T Human head data at AF=9. Further, the results show a 5% improvement

in terms of PSNR than IHTA and 8% improvement than IHTA at AF=9 for the same data. For 3T cardiac radial data (Table 4), the proposed method shows improvement 2 % improvement in terms of AP with reference to ISTA based CS and 4% improvement with reference to IHTA based CS at AF=6. The proposed method used GROG gridding and reconstructed the final images from the gridded data utilizing iterative *p*-thresholding. *p*-thresholding is an advanced version of the iterative soft-thresholding algorithm (ISTA) [16] and minimizes the non-convex functions. The use of the thresholding function encourages image sparsity, which is a key element in CS-based image reconstruction [18].

GROG is trajectory dependent and intimately maps the greatest number of samples even at lower acceleration factors in the focal point of the gridded *k*-space [9].

The efficiency of the proposed method deteriorates at higher acceleration factors as the distance between the acquired radial spokes becomes greater; thus, GROG maps fewer samples at the center of *k*-space and leaves more gaps. After gridding, CS-based iterative *p*-thresholding is used to reconstruct the artifact-free images. CS-based *p*-thresholding directly cancels the incoherent artifacts created due to the sub-sampling of k-space.

Figs. 2 to 5 show that the CS-based soft and hard-thresholding exhibit more aliasing artifacts at lower AFs compared to our proposed method. Also, the proposed technique successfully recovers the images whereas conventional CS-based soft and hard-thresholding fail to remove the artifacts at higher AF i.e., 6&9.

Evident from the quantifying parameters and visual assessment of the reconstruction results, the proposed scheme provides an improvement in AP, RMSE, and PSNR values at different acceleration factors e.g., 4, 6, and 9. Also, a visual assessment of the reconstruction results demonstrates that the proposed method has noticeably removed the artifacts whereas artifacts remain in the case of CS-based soft and hard-thresholding.

In this work, the thresholding values in equation 8 (i.e., λ and p) are selected by comparing the image quality for a range of thresholding values. Appropriate selection of p and λ is very important for efficient reconstruction. In the future, machine learning could be used for an automatic determination of the thresholding parameters in Equation 8 for efficient reconstruction results.

2. Conclusion

This paper presented GROG followed by CS-based *p*-thresholding (GROG-pCS) for partially acquired radially *k*-space data. The proposed method is assessed on 4 different MRI data sets, (i) Shepp-Logan phantom, (ii) 1.5T human head data (iii) (iii) 3T human head data and (iv) 3T short axial cardiac real-time radial data at different acceleration factors ($4 \leq AF \leq 9$). The results show that there are substantial improvements in the results of the proposed method than conventional CS-based soft and hard-thresholding algorithms e.g., the results of 1.5T brain data showed improved results, such as 50% & 88% increase in AP, 29% & 70% in RMSE, and 4% & 12% in PSNR at AF=6.

3. References

[1] McRobbie, D. W., Moore, E. A., Graves, M. J., & Prince, M. R. *MRI from Picture to Proton*. Cambridge university press, 2017.
[2] Panych, L. P., & Madore, B, . The physics of MRI safety. *Journal of Magnetic Resonance Imaging*, ***47*****(1),** 28-43(2018).
[3] K. P. Pruessmann, M. Weiger, M. B. Scheidegger, and P. Boesiger, "SENSE: Sensitivity Encoding for Fast MRI." Accessed: Mar. 02, [Online]. Available: http://macduff.usc.edu/ee591/library/Pruessmann-SENSE.pdf (2019).
[4] M. A. Griswold et al., "Generalized Autocalibrating Partially Parallel Acquisitions (GRAPPA)," Magn. Reson. Med., **47(6),** 1202–1210, doi: 10.1002/mrm.10171 (2002).
[5] M. Uecker et al., "ESPIRiT - An eigenvalue approach to autocalibrating parallel MRI: Where SENSE meets GRAPPA," Magn. Reson. Med., **71(3),** 990–1001, doi: 10.1002/mrm.24751(2014).
[6] I. Ullah, O. Inam, I. Aslam, and H. Omer, "Accelerating Parallel Magnetic Resonance Imaging Using p-Thresholding Based Compressed-Sensing," Appl. Magn. Reson., **50(1–3),** 243–261, doi: 10.1007/s00723-018-1062-6 (2019).
[7] J. I. Jackson, C. H. Meyer, D. G. Nishimura, and A. Macovski, "Selection of a convolution function for Fourier inversion using gridding (computerised tomography application)," IEEE Trans. Med. Imaging, **10(3),** 473–478, doi: 10.1109/42.97598 (1991).
[8] J. A. Fessler and B. P. Sutton, "Nonuniform fast fourier transforms using min-max interpolation," IEEE Trans. Signal Process., **51(2),** 560–574, Feb.doi: 10.1109/TSP.2002.807005 (2003).
[9] N. Seiberlich, F. A. Breuer, M. Blaimer, K. Barkauskas, P. M. Jakob, and M. A. Griswold, "Non-Cartesian data reconstruction using GRAPPA operator gridding (GROG)," Magn. Reson. Med., **58(6)**, 1257–1265, doi: 10.1002/mrm.21435 (2007).
[10]I. Aslam, F. Najeeb, and H. Omer, "Accelerating MRI Using GROG Gridding Followed by ESPIRiT for Non-Cartesian Trajectories," Appl. Magn. Reson., doi: 10.1007/s00723-017-0943-4.2107
[11]J. A. Fessler, "On NUFFT-based gridding for non-Cartesian MRI," J. Magn. Reson., **188(2),** 191–195, doi: 10.1016/j.jmr.2007.06.012 (2007).
[12]J. Hamilton, D. Franson, and N. Seiberlich, "Recent advances in parallel imaging for MRI," Prog. Nucl. Magn. Reson. Spectrosc., **101,** 71–95, Aug. doi: 10.1016/j.pnmrs.2017.04.002 (2017).
[13]M. Lustig, D. Donoho, and J. M. Pauly, "Sparse MRI: The application of compressed sensing for rapid MR imaging," Magn. Reson. Med., **58(6),** 1182–1195, doi: 10.1002/mrm.21391 (2007).
[14]T. Blumensath and M. E. Davies, "Iterative hard thresholding for compressed sensing," Appl. Comput. Harmon. Anal., **27(3),** Nov, 265–274, doi: 10.1016/J.ACHA.2009.04.002 (2009).
[15]S. R. Rajani and M. R. Reddy, "An iterative hard thresholding algorithm for CS MRI," Feb. 2012, p. 83143W, doi: 10.1117/12.911244 (2012).
[16]S. Elahi, M. kaleem, and H. Omer, "Compressively sampled MR image reconstruction using generalized thresholding iterative algorithm," J. Magn. Reson., **286,** 91–98, doi: 10.1016/j.jmr.2017.11.008 (2018).
[17]F. Bloch, "Nuclear Induction," Phys. Rev., **70(7–8),** Oct, 460–474, doi: 10.1103/PhysRev.70.460 (1946).
[18]I. Daubechies, M. Defrise, and C. De Mol, "An Iterative Thresholding Algorithm for Linear Inverse Problems with a Sparsity Constraint." Accessed: Mar. 23, [Online]. Available: https://services.math.duke.edu/~ingrid/publications/Comm_Pure_Appl_Math_57.pdf., (2019).

[19]Z. Wang, Y. Xu, and F. Dong, “A fast iterative P-thresholding algorithm for sparse reconstruction of electrical tomography,” in 2017 IEEE International Conference on Imaging Systems and Techniques (IST), doi: 10.1109/IST.2017.8261555., Oct 2017, 1-6 (2017).
[20]X. Qu, W. Zhang, D. Guo, C. Cai, S. Cai, and Z. Chen, “Iterative thresholding compressed sensing MRI based on contourlet transform,” Inverse Probl. Sci. Eng., **18,(6),** doi: 10.1080/17415977.2010.492509. Sep 2010, 737–758 (2010).
[21]X. Zhang et al., “A guaranteed convergence analysis for the projected fast iterative soft-thresholding algorithm in parallel MRI,” Med. Image Anal., **69,** doi: 10.1016/j.media.2021.101987 (2021).
[22]J. Shah, I. Qureshi, H. Omer, and A. Khaliq, “A modified POCS-based reconstruction method for compressively sampled MR imaging,” Int. J. Imaging Syst. Technol., **24(3),** doi: 10.1002/ima.22095. Sep, 203-207 (2014).
[23]S. Voronin and R. Chartrand, “A new generalized thresholding algorithm for inverse problems with sparsity constraints,” in 2013 IEEE International Conference on Acoustics, Speech and Signal Processing, doi: 10.1109/ICASSP.2013.6637929. May, 1636–1640 (2013).
[24]Gol Gungor, D., & Potter, L. C.A subspace-based coil combination method for phased-array magnetic resonance imaging. Magnetic resonance in medicine, **75(2),** 762-774 (2016).
[25] Omer, H. *Parallel MRI: tools and applications* (Doctoral dissertation, Imperial College London). 2012